Single-Component Conductors: A Sturdy Electronic Structure Generated by Bulky Substituents

Agathe Filatre-Furcate, Nathalie Bellec, Olivier Jeannin, Pascale Auban-Senzier, Marc Fourmigué, Jorgé Iñiguez, Enric Canadell, Benjamin Brière, Vinh Ta Phuoc, Dominique Lorcy

Sturdy Semiconducting State Powered by Bulky Substituents in Single-Component Conductors

Agathe Filatre-Furcate,[†] Nathalie Bellec,[†] Olivier Jeannin,[†] Pascale Auban-Senzier,[‡] Marc Fourmigué,[†] Jorge Íñiguez,[¥,§] Enric Canadell,*[,§] Benjamin Brière,[♯] Vinh Ta Phuoc,[♯] and Dominique Lorcy*[,†]

[†] *Institut des Sciences Chimiques de Rennes, UMR 6226 CNRS-Université de Rennes 1, Matière Condensée et Systèmes Electroactifs (MaCSE), Campus de Beaulieu, Bât 10A, 35042 Rennes cedex, France.*

[‡] *Laboratoire de Physique des Solides UMR 8502 CNRS-Univ. Paris-Sud, Université Paris-Saclay, F.91405 Orsay cedex, France.*

[¥] *Materials Research and Technology Department, Luxembourg Institute of Science and Technology (LIST),5 avenue des Hauts-Fourneaux, L-4362 Esch/Alzette, Luxembourg.*

[§] *Institut de Ciència de Materials de Barcelona (ICMAB-CSIC), Campus de la UAB, E-08193 Bellaterra, Spain.*

[♯] *GREMAN UMR 7347 CNRS*, Université F. Rabelais, Parc de Grandmont, 37200 Tours, France

ABSTRACT: While the introduction of large, bulky substituents such as *tert*-butyl, –$SiMe_3$ or –Si(isopropyl)$_3$ has been used recently to control the solid state structures and charge mobility of organic semiconductors, this crystal engineering strategy is usually avoided in molecular metals where a maximized overlap is thought for. In order to investigate such steric effects in single component conductors, the ethyl group of the known [Au(Et-thiazdt)$_2$] radical complex has been replaced by an isopropyl one to give a novel single component molecular conductor noted [Au(*i*Pr-thiazdt)$_2$] (*i*Pr-thiazdt: N-isopropyl-1,3-thiazoline-2-thione-4,5-dithiolate). It exhibits a very original stacked structure of crisscross molecules interacting laterally to give a truly three-dimensional network. This system is semiconducting at ambient pressure (5 S.cm^{-1}) and both transport and optical measurements evidence a slowly decreasing energy gap under applied pressure with a regime change around 1.5 GPa. In contrast with other conducting systems amenable to a metallic state under physical or chemical pressure,

the semiconducting state is stable here up to 4 GPa, a consequence of its peculiar electronic structure, with indeed a very robust direct band gap resulting from an avoided band crossing.

■ INTRODUCTION

The development of molecular semiconductors with bulky groups to specifically control the overlap interactions and associated charge mobilities has proved to be an efficient approach in organic field effect transistors. For instance, devices built with pentacenes substituted at the 6,13 positions by $–C{\equiv}C–SiR_3$ groups (as in TIPS when R = iPr)[1] exhibit improved performances. Similarly, tert-butyl groups introduced on a tetrathiafulvalene core provide high mobility materials (> 1 $cm^2\ V^{-1}\ s^{-1}$).[2] Such a strategy has not been investigated purposely in organic conductors and metals, because the steric hindrance generated by these groups can easily disrupt strong intermolecular interactions needed for large band dispersion and therefore, decreases the conductivity even if close packing is generally thermodynamically favored.[3]

For example, in mixed valence salts of metal bis(dithiolene) complexes such as $C[M(dmit)_2]$ (M = Ni, Pd and dmit = 1,3-dithiole-2-thione-4,5-dithiolate), the size and the shape of the counter ion ($C^+ = NMe_4^+$, NMe_3Et^+, $NMe_2Et_2^+$,…), even if it does not participate directly in the electronic delocalization, strongly affects the organization and interactions of the main actor, $M(dmit)_2$, and thus the physical properties.[4] Besides their use as multi component molecular conductors,[5] metal bis(dithiolene) complexes, when neutral and radical, have also been studied, but to a lesser extent, as precursors of single component molecular conductors.[6,7] The substitution scheme and the shape of the dithiolene ligands within such neutral metal bis(dithiolene) complexes can also hinder short sulfur-sulfur contacts (S•••S) leading to strong intermolecular interactions. This is true indeed with bulky ligands such as in

[M(DL-bordt)$_2$], [8] [M($S_2C_2Ph_2$)$_2$], [9] [M($S_2C_2(OC_n)_2$)$_2$] [10] (M = Au, Ni) (Chart 1). Another restriction to favorable overlap can be also a non planar structure as found in [Cu(dmdt)$_2$] where a dihedral angle of 80.29° is observed between the planes of the two TTF dithiolate ligands coordinated to the Cu ion (Chart 1).[11] Nevertheless, in this case, the ligands take an arrangement similar to the "κ-type" arrangement found in organic superconductors[12] with a close packing of the dmdt ligands allowing for a very high room temperature conductivity for this complex (110 S.cm^{-1}).[13]

Chart 1

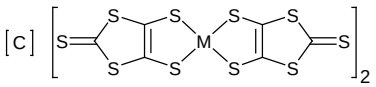

C[M(dmit)$_2$]$_2$ (M = Ni, Pd)

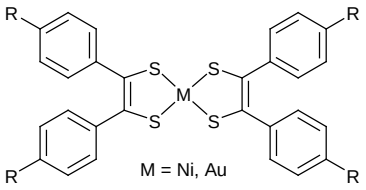

M = Ni, Au

[M($S_2C_2Ph_2$)$_2$] R = H
[M($S_2C_2(OCn)_2$)$_2$] R = OC_4H_9, $OC_{12}H_{25}$

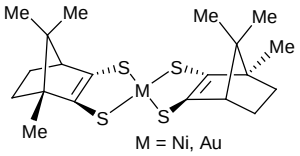

M = Ni, Au

[M(DL-bordt)$_2$]

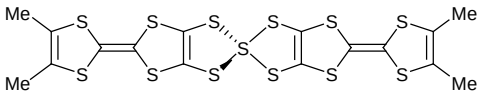

[Cu(dmdt)$_2$]

Among the various metal bis(dithiolene) complexes investigated as precursors of conducting materials, neutral gold complexes are valuable and original candidates with one radical per site, at variance with organic conductors with mixed valence character.[14,15] Along these lines, we have recently reported a single component conductor based on a neutral radical gold dithiolene complex, [Au(Et-thiazdt)$_2$] (Et-thiazdt = N-ethyl-1,3-thiazoline-2-thione-4,5-dithiolate), which behaves as a Mott insulator, with a two-dimensional layered structure (Chart 2).[16]

Chart 2

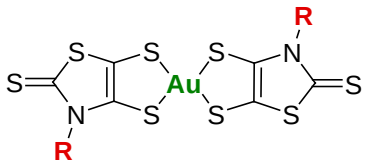

[Au(R-thiazdt)$_2$]$^{-1,0}$

R = Et[16] EtOH[18] *i*Pr

The quest for stabilizing the metallic state in this system prompted us to perform different chemical modifications of the ligand skeleton. Therefore we have successfully developed a series of neutral radical gold dithiolene complexes by replacing the outer sulfur atoms of the thiazoline-2-thione rings by oxygen atoms and/or by replacing the coordinating sulfur atom by selenium atoms.[17] Actually, these substitutions preserve the geometry and the solid state organization of the prototypical [Au(Et-thiazdt)$_2$] complex, as these compounds were all isostructural, but induce highly anisotropic chemical pressure effects, as demonstrated by the analysis of unit cell evolutions, with associated changes in conductivity. We also performed another type of structural modification of the ligand skeleton that consists in replacing the ethyl group of the thiazole ring by a hydroxyethyl one.[18] Even if the hydroxyethyl group is slightly bulkier than the ethyl one, the neutral complex [Au(EtOH-thiazdt)$_2$] proved isostructural with the previously reported examples of neutral gold dithiolene complexes belonging to the same family (Chart 2).

In order to modify the solid state organization of such radical gold complexes to a larger extend, we focused our attention on a bulkier nitrogen substituent such as an isopropyl group (R = *i*Pr). The choice of the isopropyl group is not a random selection. Indeed, it has been demonstrated that an isopropyl group connected to a thiazole core can adopt two types of conformations with in both cases one methyl above and one below the plane of the thiazole core.[19] Thus, the disposition of the additional methyl should prevent the same type of organization as the one observed for the gold complexes with an ethyl substituent or an hydroxyethyl one.

Herein we present the influence of the bulkier isopropyl group (R = *i*Pr) on the structural and electrochemical properties of the complexes as well as on the conducting properties of the corresponding materials. A very original crisscross solid state organization is found, associated with a peculiar electronic structure, which makes this compound highly resistant to physical pressure effects, at variance with earlier examples.

■ RESULTS AND DISCUSSION

Synthesis. The synthesis of the thiazoline-2-thione ring **1**[20] substituted by an isopropyl (*i*Pr) group was realized according the chemical strategy developed for other thiazoline-2-thiones starting from primary amine as outlined in Scheme 1.[21]

Scheme 1

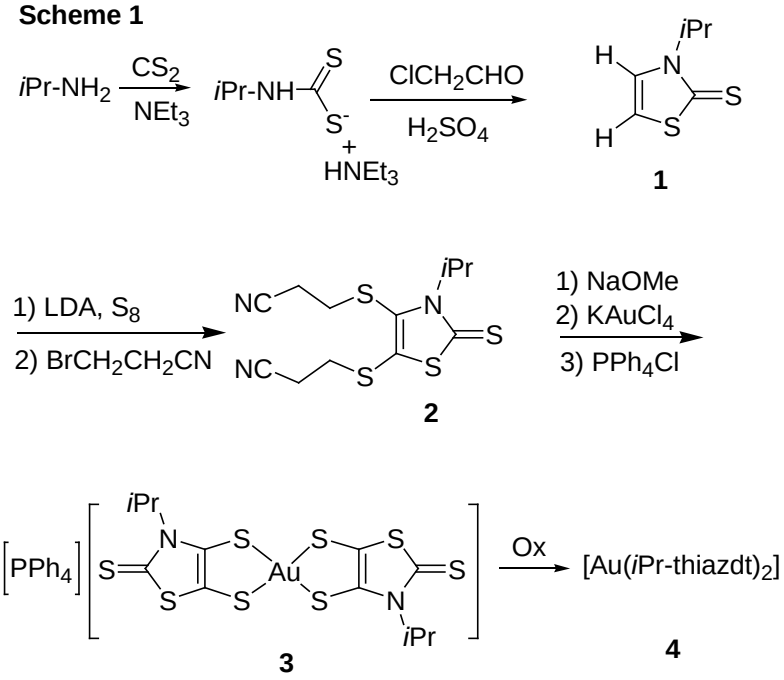

The dithiocarbamate salt was prepared by adding carbon disulfide and triethylamine to a solution of the 2-propanamine in diethylether. The reaction of chloroacetaldehyde with the dithiocarbamate salt followed by cyclisation and dehydration in the presence of sulfuric acid led to thiazoline-2-thione **1**. Formation of the protected dithiolate ligand **2** was realized through the bismetallation of **1** with LDA followed by the addition of S_8 and

bromopropionitrile (Scheme 1). The ^{1}H NMR spectrum of **2** shows some peculiarities. Indeed at room temperature it exhibits three broad signals for the isopropyl group, one at 1.76 ppm for the two CH_3 and two at 5.24 and 5.96 ppm for the C–H with an intensity ratio 6:0.5:0.5. Variable temperature ^{1}H NMR experiments performed in $CDCl_3$ were performed by decreasing the temperature by steps of 10°C. Upon lowering the temperature the methyl signal at 1.76 ppm decoalesces into two sharp doublets at 1.83 and 1.69 ppm while the two signals for the C–H gives two well resolved septuplets at 5.3 and 5.96 ppm with the intensity ratio 48:52 (Figure 1).

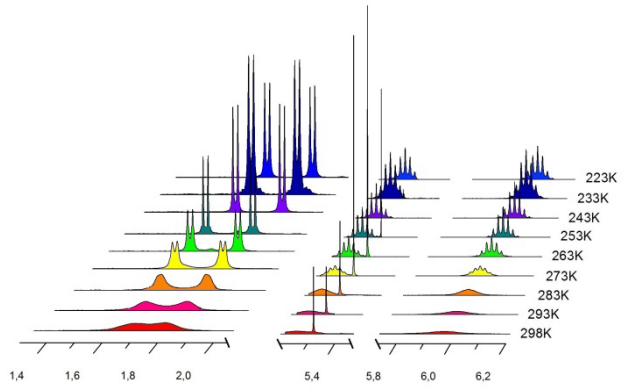

Figure 1 ^{1}H NMR spectra of the isopropyl group, C–H and CH_3 protons, of **2** at various temperature.

This observation is reminiscent of those performed by Roussel and coworkers on thiazoline analogues with an N–isopropyl group.[19] This phenomena indicates the existence of two possible rotamers due to hindered rotation of the isopropyl group, because of the presence of the cyanoethylthio groups, and thus to different orientations of the C–H of the isopropyl group relative to the thiazoline-2-thione plane. The C–H is oriented either towards the C=S bond leading to the *anti* rotamer, or towards the cyanoethylthio groups to give the *syn* rotamer (Chart 3). Contrariwise, for the unsubstituted **1**, the rotation about the N–C bond is relatively unhindered for the interconversion to occur.

Chart 3

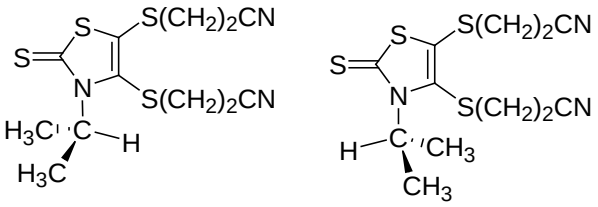

"syn" ***"anti"***

The synthesis of the monanionic gold complex **3** was realized by adding sodium methanolate to a solution of **2**, in order to deprotect the dithiolate ligand, followed by the addition of $KAuCl_4$ and PPh_4Cl. As previously observed for the ligand **2**, the ^1H NMR spectrum of **3** displays at room temperature broad signals due to the existence of rotamers. However for this gold complex only three broad signals were observed, two for the C–H at 5.74 ppm and at 4.62 ppm and one for the CH_3 at 1.58 ppm. Therefore here again the rotation of each isopropyl group can be hindered leading to the existence of different conformers: *anti*/*anti*, *syn*/*anti* and *syn*/*syn*. Furthermore, due to the presence of dissymmetrical ligands, this complex **3** is susceptible to adopt a *trans* and *cis* configuration, leading to six plausible possibilities, three conformations for each configuration (Chart 4). Temperature dependence of the ^1H NMR spectra carried out on this complex **3** shows that upon lowering the temperature, the broad signals for the C–H at 5.74 ppm and at 4.62 ppm change into two sharp multiplets, due to the superposition of two septuplets of almost equal intensity, with a ratio of 92:8. Thus, among those four distinguishable signals, two representing 92% are attributed to one rotamer *syn* or *anti* and the two others for 8% for the other rotamer in either cis or trans configuration. For the broad signal assigned to the CH_3 at 1.58 ppm, it decoalesces into two doublets at 1.60 ppm and 1.56 ppm with a ratio of 55:45 (Figure S1) and certainly due to the low amount of one of the rotamer (8%) or the superposition of the signals the four set of signals is not noted. Thus, contrary to what was observed for the precursor **2**, in the case of the dithiolene complex **3** one of the rotamer, *syn* or *anti* exists predominantly in solution.

Chart 4

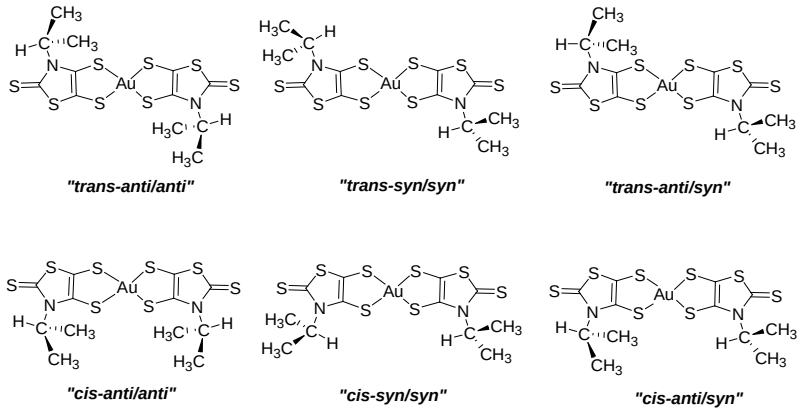

Structural and electrochemical properties. The monanionic gold complex **3** recrystallized in CH_3CN was isolated as dark green crystals and the molecular structure has been elucidated by X-ray diffraction. It crystallizes in the monoclinic system, space group C2/*c*. Selected bond lengths are collected in Table 1. The molecular structure of complex **3** (Figure 2) is characterized by a *trans* configuration and the *syn*/*syn* conformation with the two C–H of the isopropyl groups pointing towards the metallacycles. The metallacycle of this monoanionic complex is slightly distorted from planarity along the S•••S axis (5.13(7)°).

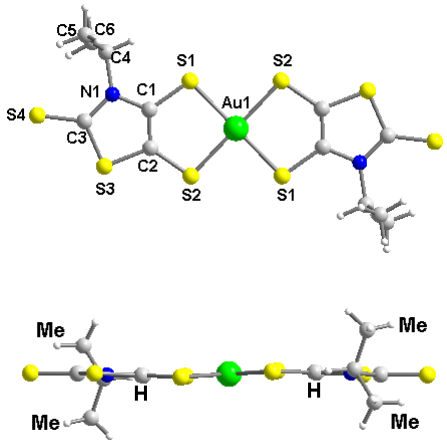

Figure 2 Molecular view (top) and side view (bottom) of the monoanionic species of the $[PPh_4][Au(i\text{Pr-thiazdt})_2]$ **3**.

Table 1 Intramolecular bond lengths (in Å) in monoanionic and neutral dithiolene complexes *trans*-[Au(*i*Pr-thiazdt)$_2$]$^{1-,\bullet}$, together with the folding angle $\theta_{S\cdots S}$ (in °) of the metallacycle along the S•••S axis.

	[Au(*i*Pr-thiazdt)$_2$]$^{1-}$	[Au(*i*Pr-thiazdt)$_2$]$^{\bullet}$ **moleculeA**	[Au(*i*Pr-thiazdt)$_2$]$^{\bullet}$ **molecule B**
Au−S1	2.3275(5)	2.3109(13)	2.3079(12)
Au−S2	2.3123(5)	2.3196(11)	2.3188(12)
S1−C1	1.754(2)	1.736(5)	1.732(5)
S2−C2	1.739(2)	1.716(5)	1.714(5)
C1−C2	1.346(3)	1.369(7)	1.366(7)
C1−N1	1.412(2)	1.385(6)	1.399(6)
C2−S3	1.741(2)	1.740(5)	1.744(5)
N1−C3	1.360(3)	1.372(6)	1.389(6)
S3−C3	1.736(2)	1.740(5)	1.733(5)
C3−S4	1.677(2)	1.658(5)	1.658(5)
$\theta_{S\cdots S}$	5.16(5)	2.15(12)	1.07(13)

Determination of the redox potentials were carried out on [PPh$_4$][Au(*i*Pr-thiazdt)$_2$] **3** by cyclic voltammetry (Figure 3) performed in CH_2Cl_2 using NBu_4PF_6 as supporting electrolyte. This dithiolene complex exhibits an irreversible reduction process at –0.95 V *vs* SCE and two reversible monoelectronic oxidation waves at E_1 = +0.52V and E_2 = +0.63 V *vs* SCE. The two oxidation processes correspond to the formation of the neutral and to the monocationic species respectively. Note that these values are very close to those found for the ethyl-substituted analog, [Au(Et-thiazdt)$_2$]$^{1-}$ (E_1 = +0.52V and E_2 = +0.65 V *vs* SCE).

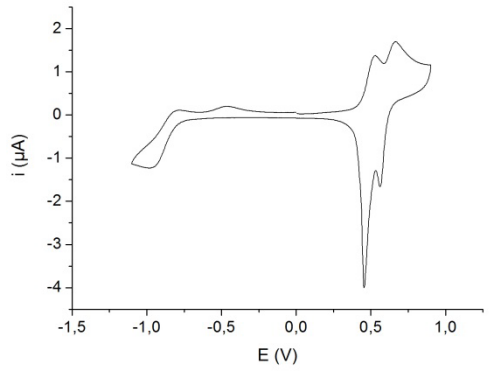

Figure 3 Cyclic voltamogram of $[Au(i\text{Pr-thiazdt})_2]^{1-}$ in CH_2Cl_2 with $[NBu_4][PF_6]$ 0.1 M as electrolyte, E in V *vs* SCE, scan rate 100 $mV.s^{-1}$.

Oxidation of this anionic complex has been realized by electrocrystallization performed in acetonitrile in the presence of NBu_4PF_6 as the supporting electrolyte upon application of a current intensity of 0.3 µA. After a couple of days, crystals of the neutral complex $[Au(i\text{Pr-thiazdt})_2]$ **4** suitable for an X-ray diffraction study were collected on the anode. It crystallizes in the monoclinic system, $P2_1/c$ space group with two crystallographic independent Au complexes, each of them located on an inversion center. The two neutral complexes, molecules A and B, are planar with very small S•••S folding angles of 2.15(12)° for Au1 and 1.07(13)° for Au2 compared to the monoanionic species (Table 1). As already observed for the monanionic species, the neutral complex derived from the coordination of two dissymmetrical dithiolene ligands adopt a *trans* configuration. Concerning the disposition of the isopropyl group with respect to the plane of the complex, the *anti*/*anti* conformation, with the two C–H of the isopropyl groups pointing towards the C=S bond of the thiazole ring, is obtained. In the solid state, the neutral complex crystallizes in a different conformation (*anti*/*anti*) than the one obtained for the monanionic species (*syn*/*syn*).

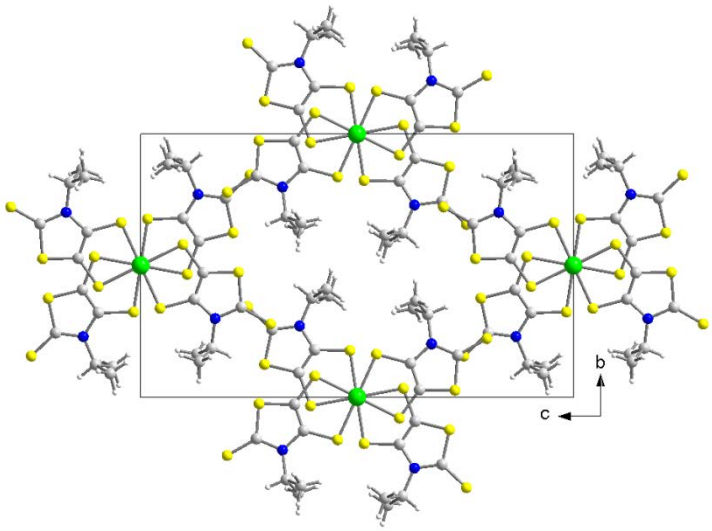

Figure 4 : Projection view along *a* of the unit cell of [Au(*i*Pr-thiazdt)$_2$] **4**.

Comparison of the bond length between the monoanionic and the neutral species, [Au(*i*Pr-thiazdt)$_2$]$^{1-,\bullet}$, shows that oxidation induces pronounced modifications on the metallacycle, with shortening of the C–S bonds and lengthening of the C=C bond, and to a lesser extent within the thiazole rings. This bond lengths evolution upon oxidation indicates the extensive delocalization of the spin density on the dithiolene moieties as already observed for other gold dithiolene complexes.[18,17,18]

The two crystallographically independent molecules A and B alternate and form uniform stacks –Au1–Au2–Au1–Au2– along *a* with a distance Au1•••Au2 of 3.483(1) Å. Due to the bulky isopropyl groups on the thiazole rings, there is now a large rotation of the long axis of the molecule with respect to each other by an angle of ≈70° (Figure 4). Within the stacks, the shortest S•••S contacts between neighboring complexes amount to 3.693(5) and 3.750(5) Å and involve the sulfur atoms of the metallacycles (Figure 5, top). Actually these distances are in the range of twice the van der Waals radius of sulfur (3.70 Å).

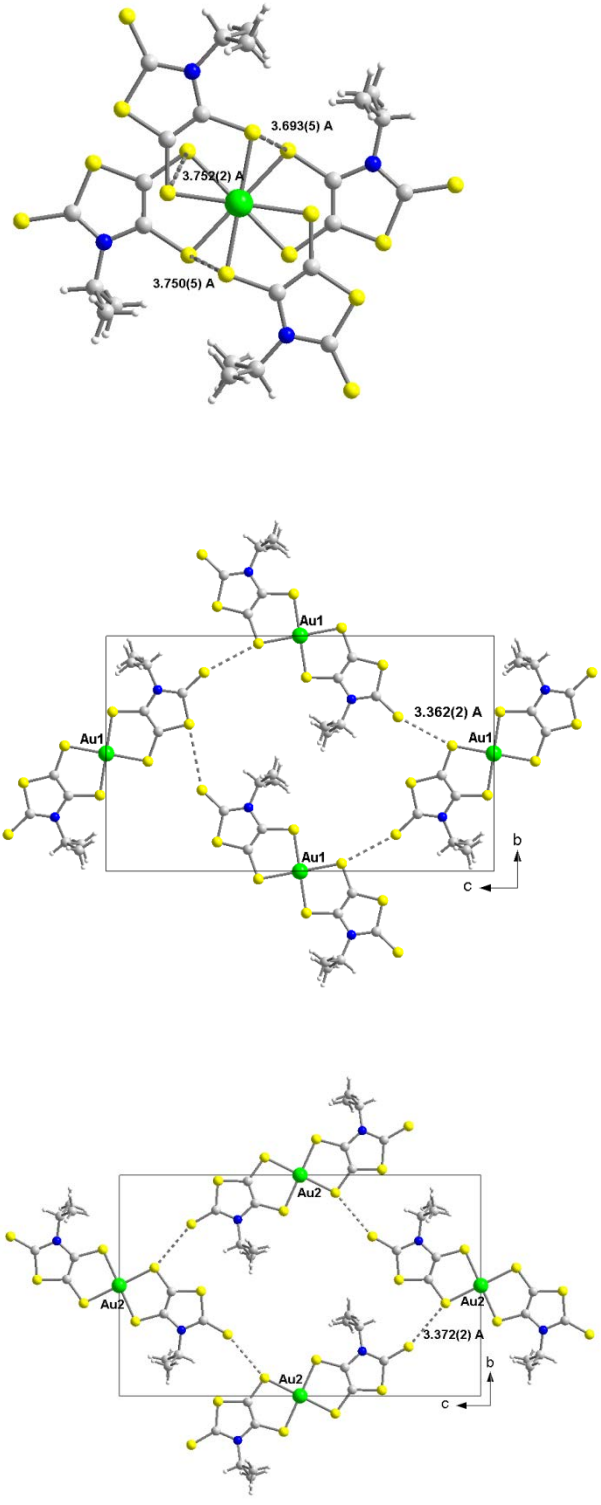

Figure 5. View of the short S•••S contacts within the stacks along the stacking axis *a* (top) and between the stacks along the *bc* plane with molecules A (Au1) (middle) and molecules B (Au2) (bottom).

As illustrated in Figure 5, much shorter intermolecular S•••S contacts (3.36–3.37 Å),

can be also observed in the *bc* plane. These S•••S contacts involve the exocyclic sulfur atom of the thiazole core and the sulfur atom of the metallacycle of two molecules A or two molecules B leading to potentially strong interactions in the *bc* plane and giving the whole structure a three-dimensional character (Figure 5).

It should be stressed here that this original crisscross structure within 1D stacks, interacting sideways in the two other perpendicular directions, completely differs from that observed in the other reported complexes belonging to the same family with R = Et or R = $(CH_2)_2OH$.[16–18] In the latter indeed, regular stacks of neutral radicals interacts only laterally to form two-dimensionnal layered structures. In other words, the steric constraints brought by the isopropyl groups in **4** limit the stacking of the radical complexes to a very specific criss-cross overlap but allow for sizeable S•••S contacts between these stacks in the two perpendicular directions.

Magnetic properties. The temperature dependence of the paramagnetic susceptibility was determined in the 2–300 K temperature range. The paramagnetic susceptibility, corrected for the Pascal diamagnetic term, (3×10^{-4} $cm^3.mol^{-1}$ at room temperature), is almost temperature independent in agreement with a Pauli-type susceptibility of a good conductor and in the same range as the one observed for [Au(Et-thiazdt)$_2$] (1.1×10^{-4} $cm^3.mol^{-1}$ at room temperature) (Figure S2). At low temperature, a Curie tail corresponds to less than 0.2 % of $S = 1/2$ species attributable to paramagnetic defaults.

Transport properties. The temperature dependence of the resistivity was measured on single crystals along the *a* stacking direction (axis of the needle) at ambient pressure and under hydrostatic pressure. The room temperature conductivity at ambient pressure, averaged on different crystals, amounts to σ(RT, 1 bar) = 5 $S.cm^{-1}$. The temperature dependence of the resistivity at ambient pressure shows a semiconducting behavior with

an activation energy, E_a = 0.058 eV as deduced from the fit of the data with a law of the type $\rho = \rho_0 \exp(E_a/kT)$ between 70 and 200 K (Figures 6 and S3 top panel).

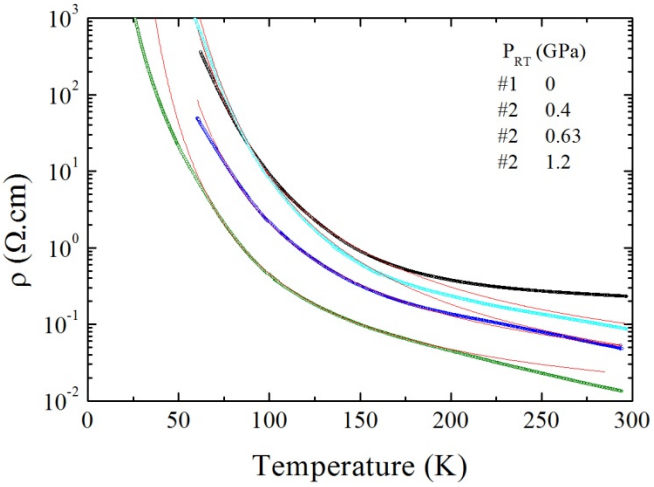

Figure 6. Temperature dependence of the resistivity of [Au(*i*Pr-thiazdt)$_2$] for sample #1 at ambient pressure and sample #2 under pressure (0.4, 0.63 and 1.2 GPa). The red lines are the Arrhenius fit to the data giving the activation energies.

The pressure dependence of the conductivity at room temperature, σ_{RT}, follows an exponential law up to 1.5 GPa (Figure 7), a further indication of a semiconducting behavior with an activation energy which varies linearly with pressure. Above 1.5 GPa however, σ_{RT} adopts a linear pressure dependence (inset of figure 7) indicating the proximity of a metallic state. By comparison, the prototypical [Au(Et-thiazdt)$_2$] complex exhibits a much higher amplitude of variation in the exponential regime σ_{RT}(1.5GPa)/ σ_{RT} (0) ~ 1000 (instead of 40 for **4**),[16] and reaches a metallic state with σ_{RT} = 1000 S.cm^{-1} at 2 GPa while for [Au(*i*Pr-thiazdt)$_2$] **4,** σ_{RT} only reaches 300 S.cm^{-1}at 2.6 GPa.

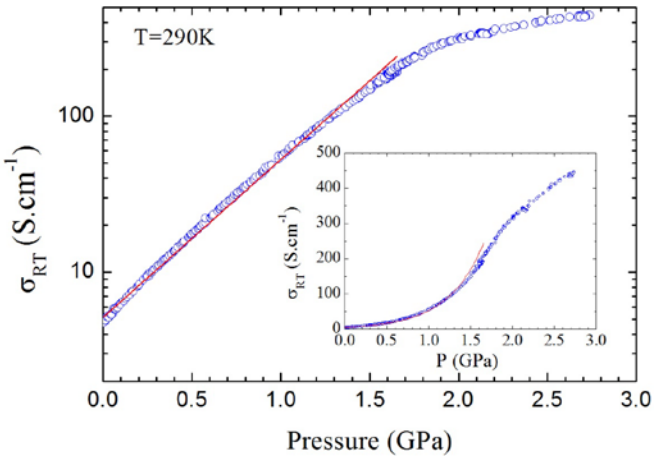

Figure 7. Pressure dependence of the room temperature conductivity of [Au(*i*Pr-thiazdt)$_2$] with a log scale in the main plot and a linear scale in the inset. The red line is an exponential fit to the data between 0 and 1.5 GPa.

This very limited effect of pressure is also evidenced on the activation energies determined from the Arrhenius fit of resistivity data. Indeed, E_a decreases from 0.058 eV at ambient pressure (or 0.065 eV at 0.4 GPa) to still 0.021 eV at 2.6 GPa (Figure S3). Note that the lower value for E_a obtained at ambient pressure compared to 0.4 GPa could be due to thermal contraction effects and that E_a is determined in a smaller temperature range (50-125 K) at high pressure (see SI for more details).

Optical Measurements. In order to complement the transport results and get a better insight on the electronic properties of **4**, optical measurements were also performed at room temperature under pressure, allowing also to reach higher pressures, up to 4.0 GPa. Optical conductivity spectra as a function of pressure are shown in Figure 8.

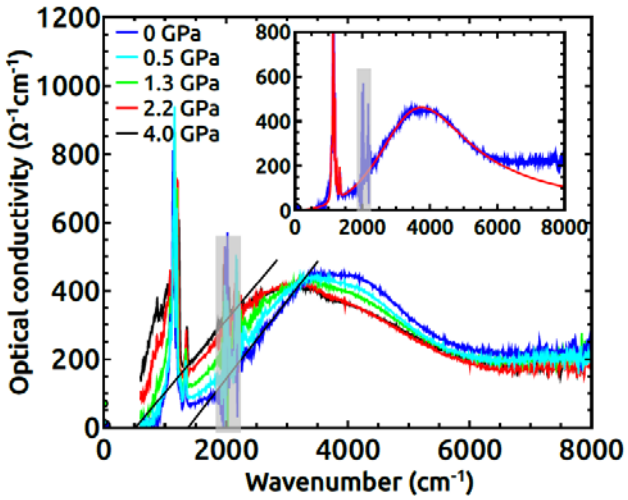

Figure 8. Optical conductivity spectra at 0, 0.5, 1.3, 2.2 and 4.0 GPa. Solid lines are the slope of the edge of the mid infrared band at 0 and 4.0 GPa (see text). Shaded area corresponds to the diamonds absorption of the anvil cell. Inset : optical conductivity at 0 Gpa. The solid line is a fit of experimental data using Lorentz oscillators.

At ambient pressure, the optical conductivity mainly consists in narrow peaks in the far infrared due to phonons, and a broad mid-infrared excitation. Apart phonon modes, the optical conductivity can roughly be fitted with a single Lorentz oscillator of width approx. 3450 cm^{-1} (0.43 eV), centered at 3760 cm^{-1} (0.46 eV) (inset of Figure 8). This latter excitation is assigned to electronic transition within SOMO bands across the Fermi level. These results are in good agreement with DFT calculations (see below). The optical gap, determined as the intersection of the slope of the edge of the mid infrared band and the x-axis, is estimated to 0.17 eV. As pressure is increased, the mid infrared band clearly shifts to lower energy by approx 0.1 eV, up to 4.0 GPa, but remains roughly the same in both shape and width. In addition, the low energy optical conductivity increases, mainly above 1.3 GPa, but no signature of a Drude peak is observed. Note that these results are consistent with transport measurements since DC conductivity increases with pressure and a metallic regime is not

reached. As shown in Figure 9, both pressure dependence and values of the gap obtained by optical measurements are in good agreement with the activation energies extracted from transport measurements. Thus, both transport and optical data exhibit a change of behavior around 1.5 GPa, indicating the vicinity of a metallic state.

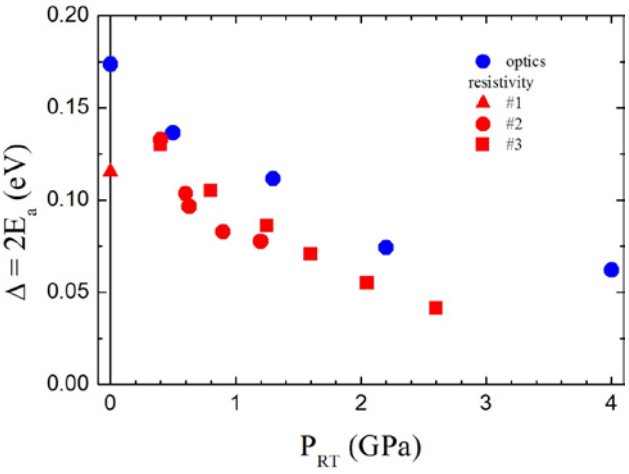

Figure 9. Pressure dependence of the gap, Δ, obtained from optical spectroscopy (blue symbols) and from transport measurements, $\Delta = 2E_a$ (red symbols).

In addition, phonons modes exhibit large changes with increasing pressure (Figure S4). Particularly, the spectral weight of mode at 1130 cm^{-1} strongly decreases with pressure and seems to disappear above 1.3 GPa. Moreover, the vibration modes around 1300 cm^{-1} are continuously screened as pressure is increased, indicating the growth of a far infrared electronic background. The optical spectral weight is roughly conserved at 6000 cm^{-1} (Figure S5) and this implies that most changes in electrodynamics properties with pressure involve an energy scale of the order of the SOMO bandwidth, as predicted by DFT calculations (see below).

In conclusion, both transport and optical measurements for **4** indicate that its semiconducting behavior is rather robust and withstands applied external pressure much better than the

prototypical ethyl-substituted complex [Au(Et-thiazdt)$_2$]. The regime change observed around 1.5 GPa stabilizes a more conductive but not fully metallic state.

Electronic structure. First-principles density functional theory (DFT) calculations were carried out to understand the transport and optical properties of this new gold dithiolene complex and the difference with those of related systems sharing the solid state organization of [Au(Et-thiazdt)$_2$].[16,17] Since [Au(*i*Pr-thiazdt)$_2$] **4** is a radical, let us first consider the different ways in which the unpaired electron of each molecule can interact in the crystal structure. As in all gold dithiolene complexes with two ligands, identical or exhibiting very small structural differences (see Table 1), the singly occupied molecular orbital (SOMO) is a π type orbital delocalized over the two ligands and with a weak participation of the gold orbitals.[16] Thus, when looking for the different ways to interact of the individual molecules, we must focus on the short contacts between the ligands. A schematic representation of the structural plot in Figure 4 is shown in Figure 10 where the molecules lying at the same height along the *a* direction are plotted with the same color. Because of the crisscross organization of successive molecules along *a*, the interactions along this direction within an individual chain (those symbolized by a blue arrow in Figure 10) may seem weaker than in the prototypical [Au(Et-thiazdt)$_2$]. However, this is not so. In the present case there are four intrachain S···S contacts of 3.693, 3.750, 3.752 and 3.802 Å whereas in [Au(Et-thiazdt)$_2$] there are only two longer S···S contacts of 3.841 Å because of the slipping of two adjacent molecules. Thus the band dispersion along the chain direction is expected to be larger in the present case. These chains are not as isolated as a quick look at the structure could suggest. As mentioned above, within the same plane, there are two S···S contacts per molecule of 3.362 or 3.372 Å depending on the plane (see Figure 5). However these contacts are of the lateral π type which is usually weak. DFT calculations for an isolated plane of molecules show that indeed they are very weak and can be disregarded in the following discussion. However, as a result of the

crisscross structure, the outer C=S bonds of a molecule at a given height fall practically on top of the outer C=S bond of a molecule of the adjacent stack lying half a unit cell below. In that way, a chain of C=S bonds almost on top of each other is generated along the *a*-direction such that every carbon atom is on top of a sulfur atom and *vice versa*. These C···S contacts are relatively short (~3.4-3.6 Å) and since the C and S p_z orbitals point almost directly toward each other, the interactions are of the strong σ type. Even if only two of the atoms of the molecule participate in one of these interactions, the excellent σ type overlap makes them very significant. These interactions are symbolized with a red arrow in Figure 10. We can thus describe the situation saying that the unpaired electrons couple tridimensionally because the different stacks interact through these chains of interactions which also run along *a* but couple neighboring chains. Equivalently, since the unpaired electron is delocalized all over the molecule, we could describe the situation saying that the chains couple because the unpaired electrons can undergo extended interactions along the crossed step-chains indicated with dashed green lines in Figure 10.

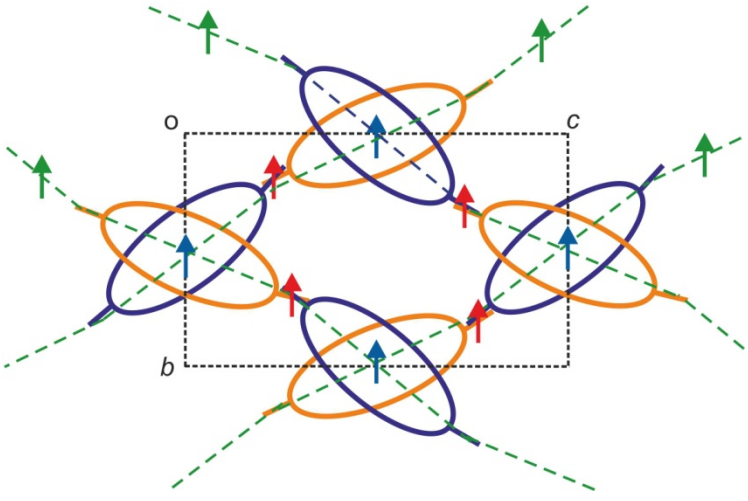

Figure 10. Schematic representation of the crystal structure of [Au(*i*Pr-thiazdt)$_2$] along *a* (see Figure 4) were the molecules at the same height are plotted with the same color. The different

types of arrows are used to indicate the different directions in which the unpaired electron of the molecule can interact (see main text).

Using the experimental crystal structure, we carried out calculations for different ways to couple the electrons in the SOMOs. We could locate two different states, a localized, non-metallic state, and a metallic one, which differ by a tiny energy difference of 2.7 meV per unit cell. Similar energy differences were previously calculated for the [Au(Et-thiazdt)$_2$] based systems.[16,17] Note that because of the usual overestimation of the stability of the metallic state in DFT, these energy differences should be taken as lower limits. The localized state is the ground state and is made of stacks with molecules with an unpaired spin up and down alternating along *a* (i.e. the blue coupling is antiferromagnetic (AFM)). The chains are coupled tridimensionally in such a way that the red couplings are ferromagnetic (FM). Localized states where the intrachain coupling is FM are higher in energy. Thus [Au(*i*Pr-thiazdt)$_2$] is predicted to be non-metallic in agreement with the resistivity measurements. The calculated band structure for this state is reported in Figure 11a (every band in this figure is actually the superposition of two bands, one associated with spin up and more localized in one every two molecules along the stacks and the other with spin down is more localized in the other set of molecules along the stack).

As noted for other gold bis(dithiolene) complexes, the single occupied molecular orbital (SOMO) and th**e** orbital immediately below (SOMO–1) differ by an energy which is not very large and must be considered in understanding the electronic structure of these molecular solids. From the eight bands in the central part of Figure 11a, the upper four (i.e. those marked with an asterisk) are mostly built from the SOMO whereas the lower four are mostly built from the SOMO–1. In contrast with the case of the [Au(Et-thiazdt)$_2$] based systems, the overlap of the two sets of bands is weak and does not play any role in determining the transport properties. In addition, the dispersion of the SOMO bands is larger in the present

case, a feature which agrees with the relatively large conductivity. In contrast, the width of the SOMO–1 bands is considerably smaller. The twist of successive molecules along the stack due to the steric requirements of the bulky isopropyl substituents leads thus to very different band structures for the present system and the [Au(Et-thiazdt)$_2$] based ones.

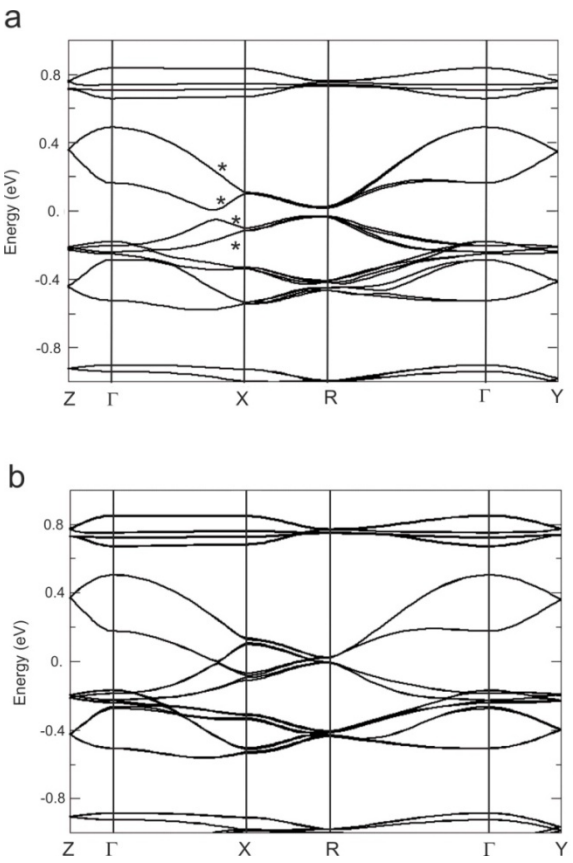

Figure 11. Band structure for the non-metallic (a) and metallic (b) states of [Au(*i*Pr-thiazdt)$_2$]. Bands marked with an asterisk are the SOMO bands. The energy zero refers to the highest occupied level of the system. Γ, X, Y, Z and R refer to the (0, 0, 0), (1/2, 0, 0), (0, 1/2, 0), (0, 0, 1/2) and (1/2, 0, 1/2) points of the monoclinic Brillouin zone.

The four SOMO bands in Figure 11a can be described as two pairs of practically folded bands along the Γ–X direction because there are two practically equivalent molecules along this direction and two equivalent stacks in the unit cell. The two upper bands have

considerably different energies at Γ and the two bands meet along the Γ-Z and Γ-Y directions, conferring an important dispersion to these bands along the directions perpendicular to the chain direction. In other words, although the coupling along the chain direction is the largest, the different chains are quite strongly coupled through the outer C=S bonds. The important feature of this band structure is that there is an avoided crossing between the second and third SOMO bands. Since only half of the SOMO bands can be filled, there is a gap separating the highest occupied and lowest unoccupied band levels and the conductivity must be activated, in agreement with the transport measurements. The calculated band structure for the metallic state is shown in Figure 11b. It is very similar to that of the non-metallic state except for the absence of the avoided crossing between the second and third SOMO bands. The origin of the avoided crossing in the nonmetallic state lies in the fact that every molecule in the antiferromagnetically coupled chain is also part of two chains of weaker but ferromagnetic interactions along the same direction. Under such conditions the crossing of the second and third SOMO bands is not allowed. In contrast, the two sets of interactions are AFM in the metallic state and the crossing is allowed. It is therefore clear that the gap resulting from this avoided crossing stabilizes the system and makes the nonmetallic state more stable.

Although both [Au(*i*Pr-thiazdt)$_2$] **4** and [Au(Et-thiazdt)$_2$] have a localized non metallic state as the ground state, the origin of this feature is completely different. In [Au(Et-thiazdt)$_2$], the band gap is an indirect gap which can disappear simply by increasing the band dispersion, something which can be easily brought about by applying pressure.[16] In contrast, the band gap for [Au(*i*Pr-thiazdt)$_2$] **4** is the consequence of an avoided crossing between two bands. As discussed above, this is a consequence of the topological properties of the lattice and the fact that the SOMO is delocalized over the dithiolene ligands. Thus, using pressure to modify the band dispersion cannot remove this gap unless the topology of the lattice is dismantled. In principle, both an increase (as it presumably occurs for [Au(Et-thiazdt)$_2$]) or decrease of the

intermolecular interactions may result from the application of pressure. However the avoided crossing must persist in both cases. As an illustration of this situation, the calculated band structure when the intermolecular distance was shortened by 0.1 Å along the chain axis (i.e. a 2.9% contraction along *a*) is show in Figure 12. As reasoned above the band gap arising from the avoided crossing is kept without much change. Consequently, an activated conductivity is expected if under pressure the essential topology of the lattice is kept or if the structure evolves to a different topology in such way that the intermolecular interactions are not strong. However the results in Figure 6 clearly argue in favor of the first possibility. Thus, in clear contrast with other single component molecular conductors, be they organic molecules (bisdithiazolyls)[22] or metal complexes (Ni(dmit)$_2$,[23] Au(Et-thiazdt)$_2$,[16]) which can be made metallic under physical or chemical pressure,[17] [Au(*i*Pr-thiazdt)$_2$] is expected to keep the nonmetallic behavior under pressure, in agreement with our transport measurements.

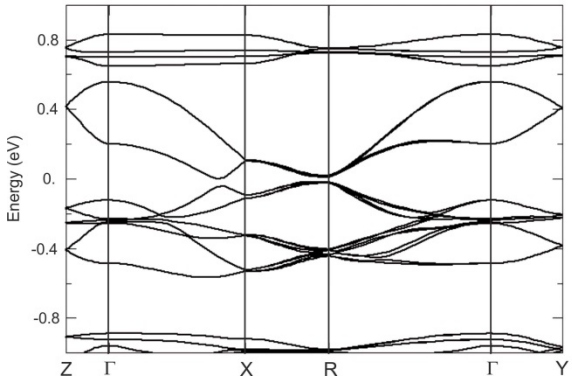

Figure 12. Band structure for the non-metallic state of [Au(*i*Pr-thiazdt)$_2$] when the molecules were rigidly brought together by 0.1 Å along the chain axis. The energy zero refers to the highest occupied level of the system.Γ, X, Y, Z and R refer to the (0, 0, 0), (1/2, 0, 0), (0, 1/2, 0), (0, 0, 1/2) and (1/2, 0, 1/2) points of the monoclinic Brillouin zone.

■ CONCLUDING REMARKS

We have reported here the influence of steric effect both on the organization and the properties of a single component molecular conductor, namely [Au(*i*Pr-thiazdt)$_2$]. Despite the presence of two bulky isopropyl groups on the planar radical gold dithiolene complex, the system has found a way to favor strong intermolecular overlap interactions by adopting an original crisscross overlap, at variance with the one observed for the prototypical [Au(Et-thiazdt)$_2$]. First-principles calculations show that the ground state of the system is nonmetallic with antiferromagnetic coupling of the SOMO electrons along the stacks but ferromagnetic coupling between the stacks. At variance with [Au(Et-thiazdt)$_2$] which exhibits an indirect band gap amenable to closing under pressure leading to a metallic state,[7,8] the isopropyl complex [Au(*i*Pr-thiazdt)$_2$] possesses a direct band gap resulting from an avoided band crossing. This symmetry constraint is maintained under applied pressure and strongly stabilizes the semiconducting behavior, as experimentally observed from transport and optical measurements.

Experimental section

General. NMR spectra were recorded at room temperature using $CDCl_3$ unless otherwise noted. Chemical shifts are reported in ppm referenced to TMS for ^{1}H NMR. High resolution mass spectrometry (HRMS) were performed using the fast bombardment (FAB) ionization mode and the (ESI) electrospray ionization mode by the Centre Régional de Mesures Physiques de l'Ouest, Rennes. CVs were carried out on a 10^{-3} M solution of complex in CH_2Cl_2-[NBu_4][PF_6] 0.1 M. Potentials were measured *versus* Saturated Calomel Electrode (SCE). Chemicals and materials from commercial sources were used without further purification.

1,3-thiazoline-2-thiones 1. At 0 °C, to a solution of isopropylamine (2.1 mL, 25 mmol) and triethylamine (3.8 mL, 27.5 mmol) in 200 mL of diethylether, CS_2 (1.7 mL, 27.5 mmol)

was slowly added. The reaction mixture was stirred for 30 minutes at 0 °C. The white solid was filtered, washed with diethyl ether and dried under vacuum. The dithiocarbamate salts are used in the next step without further purification. White powder, yield = 51% (3 g), mp = 132 °C. ^{1}H NMR (D_2O, 300 MHz) δ 1.15 (t, 9H, CH_3, $^{3}J_{HH}$ = 7.3 Hz), 1.17 (d, 6H, CH_3, $^{3}J_{HH}$ = 6.6 Hz), 3.09 (q, 6H, CH_2, $^{3}J_{HH}$ = 7.3 Hz), 4.25 (sept, 1H, CH, $^{3}J_{HH}$ = 6.6 Hz); ^{13}C NMR (D_2O, 75 MHz) δ 8.3 (CH_3),19.8 (N-CH($\underline{CH_3}$)$_2$), 46.6 (CH_2), 49.9 (N-$\underline{CH}$(CH_3)$_2$), 207.9 (C=S).

To a solution of the dithiocarbamate salt (12.8 g, 54 mmol) in acetonitrile (100 mL) chloroacetaldehyde (7.2 mL, 56.7 mmol, 50% in water) was slowly added. The pale yellow solution was stirred at room temperature overnight. The volume was reduced to about 10 mL by rotary evaporation and the brown residue was slowly added to 25 mL of concentrated sulfuric acid cooled at 0° C. The reaction mixture was stirred during 20 minutes, hydrolyzed with ice water and extracted with dichloromethane. The organic phase was washed with water, dried over $MgSO_4$ and the solvent was removed under reduced pressure to give thiazoline-2-thione **1** which was purified by column chromatography using dichloromethane as eluent. Beige powder (R_f = 0.55) , yield = 91% (4.9 g), mp = 56 °C; ^{1}H NMR (300 MHz**)** δ 1.38 (d, 6H, CH_3, $^{3}J_{HH}$ = 7.4 Hz), 5.37 (sept, 1H, CH, $^{3}J_{HH}$ = 7.4 Hz), 6.64 (d, 1H, =CH, $^{3}J_{HH}$ = 4.6 Hz), 7.12 (d, 1H, =CH, $^{3}J_{HH}$ = 4.6 Hz); ^{13}C NMR (75 MHz) δ 21.4 (CH_3), 50.3 (CH), 111.4 (=CH), 127.2 (=CH), 186.0 (C=S); HRMS calcd for $[M+H]^+$(ASAP) $C_6H_{10}NS_2$: 160.02492. Found 160.0249; Anal. Calcd for $C_6H_9NS_2$: C, 45.25; H, 5.70; N, 8.79; S, 40.26. Found : C, 45.14; H, 5.69; N, 8.80; S, 40.77.

4,5-biscyanoethylthio-1,3-thiazoline-2-thiones 2 Under inert atmosphere, at -10 °C, freshly prepared LDA (7.5 mL, 12.0 mmol) was added to a solution of 1,3-thiazoline-2-thione **1** (1.27 g, 8.0 mmol) in 40 mL of anhydrous THF. After stirring for 30 minutes at -10°C, of sulfur S_8 (0.38 g, 12.0 mmol) was added and the solution was stirred for an

additional 30 minutes. A solution of 16.0 mmol of LDA was added to the reaction medium. Stirring is continued for 3 hours, at -10°C, and 0.51 g (16.0 mmol) of sulfur was added. After 30 minutes 6.6 mL (80.0 mmol) of 3-bromopropionitrile was added and the reaction mixture was stirred overnight. The solvent was removed in vacuo and the residue was dissolved in dichloromethane. The organic phase was washed with water and then dried over $MgSO_4$. The resulting oil was purified by column chromatography using diethylether / dichloromethane as eluent (0.1/9.9). **2** was isolated as an orange oil. (R_f = 0.57), yield = 40%. For the main rotamer (52.4%) ^{1}H NMR (300 MHz**)** δ 1.69 (d, 6H, CH_3,$^3J_{HH}$ = 7.1 Hz), 2.82 (t, 4H, CH_2,$^3J_{HH}$ = 7.1 Hz), 2.91 (t, 4H, CH_2,$^3J_{HH}$ = 7.1 Hz), 5.96 (sept, 1H, CH, $^3J_{HH}$ = 7.1 Hz); ^{13}C NMR (75 MHz) δ 18.2 (N-CH($\underline{CH_3}$)$_2$), 18.5 (S-CH_2-$\underline{CH_2}$-CN), 31.6 (S-$\underline{CH_2}$-CH_2-CN), 53.4 (CH), 118.3 (CN), 126.2 (=C), 135.6 (=C), 186.9 (C=S); For the other rotamer, ^{1}H NMR (300 MHz**)** δ 1.83 (d, 6H, CH_3,$^3J_{HH}$ = 7.0 Hz), 3.07 (t, 4H, CH_2,$^3J_{HH}$ = 7.0 Hz), 3.23 (t, 4H, CH_2,$^3J_{HH}$ = 7.0 Hz), 5.30 (sept, 1H, CH, $^3J_{HH}$ = 7.0 Hz); ^{13}C NMR (75 MHz) δ 20.8 (N-CH($\underline{CH_3}$)$_2$), 18.9 (S-CH_2-$\underline{CH_2}$-CN), 33.3 (S-$\underline{CH_2}$-CH_2-CN), 56.0 (CH), 118.3 (CN), 129.0 (=C), 136.4 (=C), 187.6 (C=S); HRMS calcd for $[M]^+$(ASAP) $C_{12}H_{15}N_3S_4$: 329.01433 Found : 329.0142; Anal calcd for $C_{12}H_{13}N_3S_4$: C, 44.01; H, 4.00 ; N, 12.83. Found: C, 43.80 ; H, 3.80 ; N, 12.59.

[PPh_4][Au(iPr-thiazdt)$_2$] 3. Under inert atmosphere and at room temperature, 7 mL (7.0 mmol) of a 1M solution of sodium methanolate are added to 0.27 g (0.82 mmol) of 1,3-thiazoline-2-thione **2**. After complete dissolution of the compound, 0.19 g (0.5 mmol) of potassium tetrachloroaurate (III) hydrate ($KAuCl_4.H_2O$) dissolved in 5 mL of dry methanol is added to the reaction medium. Stirring is continued for 5 hours, 0.19 g (0.5 mmol) of tetraphenylphosphonium chloride (PPh_4Cl) dissolved in 3 mL of anhydrous methanol is added to the reaction medium. Then the reaction is stirred overnight at room temperature under argon atmosphere. The opaque dark green solution is filtered under vacuum flask. The

resulting solid is washed with methanol and recrystallized in acetonitrile. Dark green crystals, yield = 38% (150 mg), mp = 226 °C. ^{1}H NMR at room temperature (300 MHz) δ 1.58 (broad signal, 6H, CH_3), 4.62 (broad signal, 2H, CH, 8%), 5.74 (broad signal, 2H, CH, 92%), 7.61 (m, 8H, CH_{Ar}), 7.76 (m, 8H, CH_{Ar}), 7.89 (m, 4H, CH_{Ar}); HRMS calcd for [$2C^+$, A^-] (ESI) for $C_{60}H_{54}N_2P_2S_8Au$: 1317.1188. Found: 1317.1187. Anal calcd for $C_{36}H_{34}N_2PS_8$: C, 44.16; H, 3.50; N, 2.86. Found: C, 43.98; H, 3.52; N, 2.80.

Electrocrystallization. Crystals of [Au(iPr-thiazdt)$_2$] were prepared electrochemically using a two compartments cell (12 mL) with Pt electrodes. An acetonitrile solution of [PPh_4][Au(iPr-thiazdt)$_2$] (8 mg) and *n*Bu_4NPF_6 (100 mg) was placed in the anodic compartment, and an acetonitrile solution of *n*Bu_4NPF_6 (100 mg) in the cathodic compartment. Black needles of [Au(iPr-thiazdt)$_2$], were collected on the anode upon application of a constant current of 0.4 μA for 10 days.

Crystallography. Single-crystal diffraction data were collected on APEXII, Bruker-AXS diffractometer, Mo-Kα radiation (λ = 0.71073 Å) for all compounds. The structures were solved by direct methods using the *SIR97* program[24], and then refined with full-matrix least-square methods based on F^2 (*SHELXL-97*)[25] with the aid of the *WINGX*[26] program. All non-hydrogen atoms were refined with anisotropic atomic displacement parameters. H atoms were finally included in their calculated positions. Details of the final refinements are given In Table 2. The crystal structure of **3** was refined with one extra water molecule, located close to the inversion centre, with a 0.5 occupation parameter.

Resistivity measurements. The resistivity measurements were performed along the long axis of the needles (*a* crystallographic axis) of [Au(iPr-thiazdt)$_2$]. Gold pads were evaporated on the crystals in order to improve the quality of the contacts andgold wires were glued with silver paste on those contacts. Then a standard four points technique was used with

a low frequency lock-in detection (I_{ac} = 1 μA) for measured resistances below 10 kΩ and dc measurement for higher resistances (I_{dc} = 0.1-1μA).

Resistivity measurements were also performed under high hydrostatic pressure in a CuBe clamped cell up to 1.2 GPa (#2) and a NiCrAl clamped cell up to 2.6 GPa (#3) with silicon oil (Daphne 7373) as the pressure transmitting medium. The pressure at room temperature was extracted from the resistance of a manganin gauge in the pressure cell and it is this value which is indicated in the figures. However, the loss of pressure during cooling is estimated to 0.2 GPa, slightly decreasing with pressure. For experiments in the CuBe pressure cell, low temperatures have been provided by a cryocooler equipment down to 25 K with a copper-constantan thermocouple inside the pressure cell as the thermometer. For experiments in the NiCrAl pressure cell, a home-made cryostat equipped with a 4K pulse tube has been used with a cernox thermometer located outside the pressure cell. Cooling and warming curves (performed at about 0.4K/min down to 50K) have been averaged in order to annihilate the temperature gradient (0 to 10K) between the sample and the thermometer.

Optical Measurements. Ambient pressure near normal incidence reflectivity spectra were measured between 600 cm^{-1} and 10000 cm^{-1} on a 40 X 40 μm^2 surface of a [Au(*i*Pr-thiazdt)$_2$] single crystal. Measurements were obtained by using a homemade high-vacuum microscope including a X15 Schwarzchild objective connected to a BRUKER IFS 66v/S Fourier-transform spectrometer. A gold mirror was taken as reference. The high-P study was performed using a diamond anvil cell (DAC). The [Au(*i*Pr-thiazdt)$_2$] single crystal was loaded inside the gasket hole together with KBr as the hydrostatic medium. Great care was taken to obtain a clean sample-diamond interface where the reflectivity spectra, R_{sd}, was measured from 600 cm^{-1} to 10000 cm^{-1}. The gasket was taken as a reference. In order to reliably estimate the pressure-dependent optical conductivity, the R_{sd} measured in the DAC were

renormalized by a P-independent factor, by using ambient pressure measurement according to a described procedure.[27] Optical conductivity spectra were obtained by Variational Dielectric Function analysis (VDF).[28]

Computational details. We have used the spin-polarized Generalized Gradient Approximation[29] (σ-GGA) approach to Density Functional Theory[30] (DFT) as implemented in the *Vienna Ab Initio Simulation Package* (VASP).[31] We used the Projector Augmented Wave[32] method to represent the ionic cores, solving explicitly for the following electrons: 5*d* and 6*s* of Au, 3*s* and 3*p* of S, 2*s* and 2*p* of N and C, and 1*s* of H. Electronic wave functions were represented with a plane wave basis truncated at 400 eV. A careful convergence test for Brillouin Zone integrations was necessary. Accurate energy differences between various (e.g., antiferromagnetic *vs* metallic) electronic solutions were obtained using Γ-centered 4×8×4 *k*-point grids for the simulation cell with 4 molecules in it.

Table 2 Crystallographic data

	3	**4**
Formulae	$C_{36}H_{36}AuN_2OPS_8$	$C_{12}H_{14}AuN_2S_8$
FW ($g.mol^{-1}$)	997.08	639.70
System	monoclinic	monoclinic
Space group	C2/c	$P2_1/c$
a (Å)	29.0982(7)	6.9668(6)
b (Å)	7.3725(2)	12.8949(10)
c (Å)	22.3171(5)	21.2391(13)
α (deg)	90	90
β (deg)	125.1210(10)	92.757(4)
γ (deg)	90	90
V ($Å^3$)	3915.97(17)	1905.8(2)
T (K)	150(2)	150(2)
Z	4	4
D_{calc} ($g.cm^{-1}$)	1.688	2.229
μ (mm^{-1})	4.257	8.593
Total refls	29144	4337
Abs corr	multiscan	multiscan
Uniq refls (R_{int})	4485 (0.0227)	4337 (0.0409)
Uniq refls ($I > 2\sigma(I)$)	4087	3133
R_1, wR_2	0.0169, 0.039	0.0315, 0.0596
R_1, wR_2 (all data)	0.020, 0.0406	0.0532, 0.0645
GOF	1.05	1.067

Acknowledgements

We thank the CDIFX (Rennes) for access to the X-ray diffraction facilities and the ANR (France) for financial support through project n°12-BS07-0032. Work in Bellaterra was supported by MINECO (Spain) through Grant FIS2012-37549-C05-05 and Generalitat de Catalunya (2014SGR301). J.I. was financially supported by the Fond National de Recherche

Luxembourg through a PEARL grant (FNR/P12/4853155/Kreisel) and by MINECO-Spain (Grant No. MAT2013-40581-P). E.C. acknowledges support of the Spanish MINECO through the Severo Ochoa Centers of Excellence Program under Grant SEV-2015-0496.

Supporting Information Available

Additional resistivity and optical measurements figures and X-ray crystallographic files in CIF format. This material is available free of charge via the Internet at http://pubs.acs.org.

References

1 Sheraw, C. D.; Jackson, T. N.; Eaton, D. L.; Anthony, J. E. *Adv. Mater*. **2003**, *15*, 2009–2011.

2 (a) Kanno, M.; Bando, Y.; Shirahata, T.; Inoue, J.; Wada, H.; Mori, T. *J. Mater. Chem.* **2009**, *19*, 6548–6555. (b) Inoue, J.; Kanno, M.; Ashizawa, M.; Seo, C.; Tanioka, A.; Mori, T. *Chem. Lett*. **2010**, *39*, 538–540. (c) Nagakubo, J.; Ashizawa, M.; Kawamoto, T.; Tanioka, A.; Mori, T. *Phys. Chem. Chem. Phys*. **2011**, *13*, 14370–14377. (d) Higashino, T.; Akiyama, Y.; Kojima, H.; Kawamoto, T.; Mori, T. *Crystals* **2012**, *2*, 1222–1238.

3 (a) Roy, S.; Banerjee, R.; Nangia, A.; Kruger, G. J. *Chem. Eur. J.* **2006**, *12*, 3777−3788. (b) Desiraju, G. R. *Angew. Chem., Int. Ed.* **2007**, *46*, 8342−8356. (c) Desiraju, G. R. *J. Am. Chem. Soc.* **2013**, *135*, 9952−9967.

4 (a) Kato, R. *Bull. Chem. Soc. Jpn*. **2014**, *87*, 355−374. (b) Kato, R. *Chem. Rev.* **2004**, *104*, 5319−5346.

5 (a) Robertson, N.; Cronin, L. *Coord. Chem. Rev.* **2002**, *227*, 93−127. (b) Canadell, E. *Coord. Chem. Rev.* **1999**, *185-186*, 629−651. (c) Pullen, A. E.; Olk, R.-M. *Coord. Chem. Rev.* **1999**, *188*, 211−262. (d) Cassoux, P.; Valade, L.; Kobayashi, H.; Kobayashi, A.; Clark, R. A. Underhill, A. E. *Coord. Chem. Rev*. **1991**, *110*, 115−160.

6 Garreau-de Bonneval, B.; Moineau-Chane Ching, K. I.; Alary, F.; Bui, T.-T.; Valade, L. *Coord. Chem. Rev*. **2010**, *254*, 1457−1467.

7 (a) Kobayashi, A.; Fujiwara, E.; Kobayashi, H. *Chem. Rev*. **2004**, *104*, 5243−5264. (b) Cui, H.; Kobayashi, H.; Ishibashi, S.; Sasa, M.; Iwase, F.; Kato, R.; Kobayashi, A. *J. Am. Chem. Soc.* **2014**, *136*, 7619–7622. (c) Zhou, B.; Idobata, Y.; Kobayashi, A.; Cui, H.; Kato, R.; Takagi, R.; Miyagawa, K.; Kanoda, K.; Kobayashi, H. *J. Am. Chem. Soc.* **2012**, *134*, 12724–12731. (d) Cui, H.; Brooks, J. S.; Kobayashi, A.; Kobayashi, H. *J. Am. Chem. Soc.* **2009**, *131*, 6358–6359. (e) Kobayashi, A.; Tanaka, H.; Kumasaki, M.; Torii, H.; Narymbetov, B.; Adachi, T. *J. Am. Chem. Soc.* **1999**, *121*, 10763–10771. (f) Tanaka, H.; Okano, Y.; Kobayashi, H.; Suzuki, W.; Kobayashi, A. *Science* **2001**, *291*, 285−287.

8 Perochon, R.; Poriel, C.; Jeannin, O.; Piekara-Sady, L.; Fourmigué, M. *Eur. J. Inorg. Chem.* **2009**, 5413–5421.

9 (a) Megnamisi-Belombe, M.; Nuber, B. *Bull. Chem. Soc. Jpn*. **1989**, *62*, 4092−4094. (b) Miao, Q.; Gao, J.; Wang, Z.; Yu, H.; Luo, Y.; Ma, T. *Inorg. Chim. Acta* **2011**, *367*, 619−627. (c) Papavassiliou, G. C.; Anyfantis, G. C.; Raptopoulou, C. P.; Psycharis, V.; Ioannidis, N.; Petrouleas, V.; Paraskevopoulou, P. *Polyhedron* **2009**, *28*, 3368−3372.

10 Perochon, R.; Piekara-Sady, L.; Jurga, W.; Clérac, R.; Fourmigué, M. *Dalton Trans.*, **2009**, 3052–3061.

11 Tanaka, H.; Kobayashi, H.; Kobayashi, A. *J. Am. Chem. Soc*. **2002**, *124*, 10002−10003.

12 Williams, J. M.; Ferrarao, J. R.; Thorn, J. R.; Carlson, K. D.; Geiser, U.; Wang, H. H.; Kini, A. M.; Whangbo, M. *Organic Superconductors* Prentice Hall: Englewood Cliffs, New Jersey, 1992.

13 Zhou, B.; Idobata, Y.; Kobayashi, A.; Cui, H.; Kato, R.; Takagi, R.; Miyagawa, K.; Kanoda, K.; Kobayashi, H. *J. Am. Chem. Soc.* **2012**, *134*, 12724−12731.

14 (a) Okano, Y.; Zhou, B.; Tanaka, H.; Adachi, T.; Ohishi, Y.; Takata, M.; Aoyagi, S.; Nishibori, E.; Sakata, M.; Kobayashi A.; Kobayashi, H. *J. Am. Chem. Soc.* **2009**, *131*, 7169–7174. (b) Zhou, B.; Shimamura, M.; Fujiwara, E.; Kobayashi, A.; Higashi, T.; Nishibori, E.; Sakata, M.; Cui, H.; Takahashi, K.; Kobayashi, H. *J. Am. Chem. Soc.* **2006**, *128*, 3872–3873. (c) Suzuki, W.; Fujiwara, E.; Kobayashi, A.; Fujishiro, Y.; Nishibori, E.; Takata, M.; Sakata, M.; Fujiwara, H.; Kobayashi, H. *J. Am. Chem. Soc.* **2003**, *125*, 1486–1487.

15 (a) Schiødt, N. C.; Bjørnholm, T.; Bechgaard, K.; Neumeier, J. J.; Allgeier, C.; Jacobsen, C. S.; Thorup, N. *Phys. Rev. B* **1996**, *53*, 1773-1778. (b) Belo, D.; Alves, H.; Lopes, E. B.; Duarte, M. T.; Gama, V.; Henriques, R. T.; Almeida, M.; Pérez-Benítez, A.; Rovira, C.; Veciana, J. *Chem. Eur. J.* **2001**, *7*, 511−519. (c) Dautel, O. J.; Fourmigué, M.; Canadell, E.; Auban-Senzier, P. *Adv. Funct. Mater.* **2002**, *12*, 693−698.

16 Tenn, N.; Bellec, N.; Jeannin, O.; Piekara-Sady, L.; Auban-Senzier, P.; Íñiguez, J.; Canadell, E.; Lorcy, D. *J. Am. Chem. Soc.* **2009**, *131*, 16961–16967.

17 Yzambart, G.; Bellec, N.; Ghassan, N.; Jeannin, O.; Roisnel, T.; Fourmigué, M.; Auban-Senzier, P.; Íñiguez, J.; Canadell, E.; Lorcy D. *J. Am. Chem. Soc.* **2012**, *134*, 17138−17148.

18 Le Gal, Y.; Roisnel, T.; Auban-Senzier, P.; Guizouarn, T.; Lorcy D. *Inorg. Chem.* **2014**, *53*, 8755−8761.

19 Roussel, C.; Chanon, M.; Metzger, J. *Tetrahedron Lett.* **1972**, *36*, 3843−3846. (b) Roussel, C.; Lidén, A.; Chanon, M.; Metzger, J.; Sandström, J. *J. Am. Chem. Soc.* **1976**, *98*, 2847−2852.

20 Roussel, C. M.; Gallo, R.; Chanon, M.; Metzger, J. *Bull. Soc. Chim. Fr.***1971**, 1902−1907.

21 (a) Guérin, D.; Carlier, R.; Lorcy, D. *J. Org. Chem.* **2000**, *65*, 6069−6072. (b) Bellec, N. ;Lorcy, D.; Boubekeur, K.; Carlier, R.; Tallec, A.; Los, Sz.; Pukacki, W.; Trybula, M.;

Piekara-Sady, L.; Robert. A. *Chem. Mater*. **1999**, *11*, 3147−3153. (c) Bellec, N.; Lorcy, D.; Robert, A; Carlier, R.; Tallec, A.; Rimbaud, C.; Ouahab, L.; Clerac, R.; Delhaes, P. *Adv. Mater*. **1997**, *9*, 1052−1056.

22 Wong, J. W. L.; Mailman, A.; Lekin, K.; Winter, S. M.; Yong, W.; Zhao, J.; Garimella, S. V.; Tse, J. S.; Secco, R. A.; Desgreniers, S.; Ohishi, Y.; Borondics, F.; Oakley, R. T. *J. Am. Chem. Soc.* **2014**, *136*, 1070-1081.

23 Cui, H.-B.; Tsumuraya, T.; Miyazaki, T.; Okano, Y.; Kato, R. *Eur. J. Inorg. Chem.* **2014**, *24*, 3837–3840.

24 Altomare, A.; Burla, M. C.; Camalli, M.; Cascarano, G.; Giacovazzo, C.; Guagliardi, A.; Moliterni, A. G. G.; Polidori, G.; Spagna, R. *J. Appl. Cryst.* **1999**, *32*, 115−119.

25 Sheldrick G.M. *Acta Cryst*. **2008**, *A64*, 112−122.

26 Farrugia, L. J. *J. Appl. Crystallogr.* **1999**, *32*, 837–838.

27 Sacchetti, A.; Arcangeletti, E.; Perucchi, A.; Baldassarre, L.; Postorino, P.; Lupi, S.; Ru, N.; Fisher, I. R.; Degiorgi, L. *Phys. Rev. Lett.* **2007**, *98*, 026401-1–026401-4.

28 Kuzmenko, A. B. *Rev. Sci. Instrum*. **2005**, *76*, 083108-1–083108-9.

29 Perdew, J.P.; Burke, K.; Ernzerhof, M. *Phys. Rev. Lett.***1996**, *77*, 3865−3868.

30 (a) Hohenberg, P; Kohn, W. *Phys. Rev.* **1964**, *136*, B864. (b) Kohn, W.; Sham, L.J. *Phys. Rev.***1965**, *140*, A1133.

31 Kresse, G.; Furthmuller, J. *Phys. Rev. B* **1996**, *54*, 11169−11186.

32 (a) Blochl, P.E. *Phys. Rev B* **1994**, *50*, 17953−17979. (b) Kresse, G.; Joubert, D. *Phys. Rev. B* **1999**, *59*, 1758−1775.

Graphical abstract

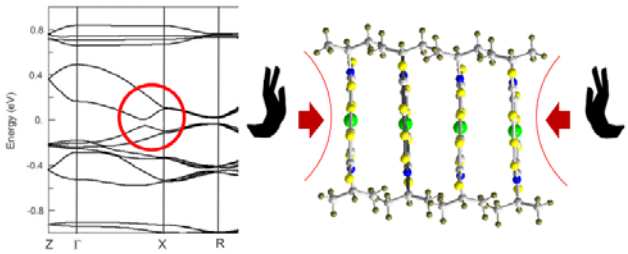

Synopsis

Introduction of bulky isopropyl groups in the single component molecular conductor [Au(*i*Pr-thiazdt)$_2$] induces a very original crisscross stacked structure exhibiting a semiconducting state stable up to 4 GPa due to a peculiar electronic structure.